Smart and Environmentally Friendly Winter Maintenance Solutions for Safe Winter Mobility: Use of a Microwave Method to Prototype Electrically Conductive Concrete

FINAL PROJECT REPORT

by

Somayeh Nassiri, PhD
Washington State University

Sponsorship
PacTrans and Washington State University

for

Pacific Northwest Transportation Consortium (PacTrans)
USDOT University Transportation Center for Federal Region 10
University of Washington
More Hall 112, Box 352700
Seattle, WA 98195-2700

In cooperation with U.S. Department of Transportation, Office of the Assistant Secretary for Research and Technology (OST-R)

Disclaimer

The contents of this report reflect the views of the authors, who are responsible for the facts and the accuracy of the information presented herein. This document is disseminated under the sponsorship of the U.S. Department of Transportation's University Transportation Centers Program, in the interest of information exchange. The Pacific Northwest Transportation Consortium, the U.S. Government and matching sponsor assume no liability for the contents or use thereof.

Technical Report Documentation Page

1. Report No.	2. Government Accession No.	3. Recipient's Catalog No.
	01701490	

4. Title and Subtitle:	5. Report Date : 05/04/2021
Smart and Environmentally Friendly Winter Maintenance Solutions for Safe Winter Mobility: Use of a Microwave Method to Prototype Electrically Conductive Concrete	6. Performing Organization Code

7. Author(s) and Affiliations:	8. Performing Organization Report No.
Abdullah Moman, MS student, Washington State University Somayeh Nassiri, 0000-0001-5367-2167, Assistant Professor, Washington State University	2018-S-WSU-3

9. Performing Organization Name and Address	10. Work Unit No. (TRAIS)
PacTrans Pacific Northwest Transportation Consortium University Transportation Center for Federal Region 10 University of Washington More Hall 112 Seattle, WA 98195-2700	11. Contract or Grant No. 69A3551747110

12. Sponsoring Organization Name and Address	13. Type of Report and Period Covered
United States Department of Transportation Research and Innovative Technology Administration 1200 New Jersey Avenue, SE Washington, DC 20590	8/16/2018 – 8/15/2020 14. Sponsoring Agency Code

15. Supplementary Notes

Report uploaded to: www.pactrans.org

16. Abstract

Electrically conductive pavement materials have shown potential as self-deicing pavements under passed electrical current. In this project, a method using microwaves was used to evaluate the electrical conductivity of pavement materials for the purpose of melting snow and ice and reducing the need for sanding and salting in the winter. The preliminary experiments in this study found the potential of the method to detect conductive mixes. The prototyped electrically conductive concrete (ECC) assessed in this study contained 0.2 and 0.3 percent weight of carbon fibers. Concentrations of 0.2 and 0.3 percentage by weight (wt%) resulted in more conductivity than a neat mix, while a decline in conductivity at 28 days was obtained for 0.4 wt%,indicating a potential percolation limit of between 0.3 and 0.4 wt%. The small samples and the quick, nondestructive method of measurement can be used to easily identify the optimum dosage and percolation limits of various conductive fibers for ECC development. Future investigations may include using this method to further determine the best fiber content to optimize electrical-thermal performance with maximum mechanical properties and durability.

17. Key Words	18. Distribution Statement
Self-deicing pavements, electrically conductive concrete	

19. Security Classification (of this report)	20. Security Classification (of this page)	21. No. of Pages	22. Price
Unclassified.	Unclassified.	55	N/A

Form DOT F 1700.7 (8-72) **Reproduction of completed page authorized**

.

SI* (Modern Metric) Conversion Factors

APPROXIMATE CONVERSIONS TO SI UNITS				
Symbol	**When You Know**	**Multiply By**	**To Find**	**Symbol**
		LENGTH		
in	inches	25.4	millimeters	mm
ft	feet	0.305	meters	m
yd	yards	0.914	meters	m
mi	miles	1.61	kilometers	km
		AREA		
in^2	square inches	645.2	square millimeters	mm^2
ft^2	square feet	0.093	square meters	m^2
yd^2	square yard	0.836	square meters	m^2
ac	acres	0.405	hectares	ha
mi^2	square miles	2.59	square kilometers	km^2
		VOLUME		
fl oz	fluid ounces	29.57	milliliters	mL
gal	gallons	3.785	liters	L
ft^3	cubic feet	0.028	cubic meters	m^3
yd^3	cubic yards	0.765	cubic meters	m^3
	NOTE: volumes greater than 1000 L shall be shown in m^3			
		MASS		
oz	ounces	28.35	grams	g
lb	pounds	0.454	kilograms	kg
T	short tons (2000 lb)	0.907	megagrams (or "metric ton")	Mg (or "t")
		TEMPERATURE (exact degrees)		
°F	Fahrenheit	5 (F-32)/9 or (F-32)/1.8	Celsius	°C
		ILLUMINATION		
fc	foot-candles	10.76	lux	lx
fl	foot-Lamberts	3.426	$candela/m^2$	cd/m^2
		FORCE and PRESSURE or STRESS		
lbf	poundforce	4.45	newtons	N
lbf/in^2	poundforce per square inch	6.89	kilopascals	kPa

APPROXIMATE CONVERSIONS FROM SI UNITS				
Symbol	**When You Know**	**Multiply By**	**To Find**	**Symbol**
		LENGTH		
mm	millimeters	0.039	inches	in
m	meters	3.28	feet	ft
m	meters	1.09	yards	yd
km	kilometers	0.621	miles	mi
		AREA		
mm^2	square millimeters	0.0016	square inches	in^2
m^2	square meters	10.764	square feet	ft^2
m^2	square meters	1.195	square yards	yd^2
ha	hectares	2.47	acres	ac
km^2	square kilometers	0.386	square miles	mi^2
		VOLUME		
mL	milliliters	0.034	fluid ounces	fl oz
L	liters	0.264	gallons	gal
m^3	cubic meters	35.314	cubic feet	ft^3
m^3	cubic meters	1.307	cubic yards	yd^3
		MASS		
g	grams	0.035	ounces	oz
kg	kilograms	2.202	pounds	lb
Mg (or "t")	megagrams (or "metric ton")	1.103	short tons (2000 lb)	T
		TEMPERATURE (exact degrees)		
°C	Celsius	1.8C+32	Fahrenheit	°F
		ILLUMINATION		
lx	lux	0.0929	foot-candles	fc
cd/m^2	$candela/m^2$	0.2919	foot-Lamberts	fl
		FORCE and PRESSURE or STRESS		
N	newtons	0.225	poundforce	lbf
kPa	kilopascals	0.145	poundforce per square inch	lbf/in^2

*SI is the symbol for the International System of Units. Appropriate rounding should be made to comply with Section 4 of ASTM E380.
(Revised March 2003)

Table of Contents

List of Figures

List of Tables

List of Abbreviations

CaC12	Calcium chloride
CNT	Carbon nanotube
ECC	Electrically conductive concrete
MgC12	Magnesium chloride
MIP	Mercury intrusion porosimetry
MWCNT	Multi-walled carbon nanotube
MUT	Material under testing
NaC1	Sodium chloride
NDT	Nondestructive testing
NMR	Nuclear magnetic resonance
NRW	Nicholson-Ross-Weir conversion method
PacTrans:	Pacific Northwest Transportation Consortium
RCF	Recycles carbon fiber
S/m	Siemens/meter
SWCNT	Single-walled carbon nanotube
TRL	Through-reflect-line
VCF	Virgin carbon fiber
VNA	Vector Network Analyzer
w/c	Water-to-cement ratio
WSDOT:	Washington State Department of Transportation

Acknowledgments

Funding for this research was provided by a grant from the Pacific Northwest Transportation Consortium (PacTrans), USDOT Transportation Center for Federal Region 10. The matching funds were provided by Washington State University.

We express our sincere gratitude to Dr. Reza Zoughi, professor, and Mr. Mathew Dvorsky, graduate student, of electrical computer engineering at Iowa State University and Dr. Deuk Heo, professor, and Mr. Aminul Aunik, graduate student, from Washington State University. All these individuals were generous with their time, responded to our questions and requests for information, and advised us on the microwave measurement unit set-up, its calibration, and data processing

.

Executive Summary

In cold areas of the United States, large amounts of salt, abrasives, and chemical deicers are applied on road surfaces for ice and snow control. The heavy use of various kinds of deicers has proved to have undesirable implications for natural and built environments. These operations are costly, they require a large amount of equipment, personnel, and vast areas for storage, and they require cleaning and sweeping operations in the spring. Recent research has shown that electrically conductive concrete (ECC) pavements can melt surface ice and snow when an electric current is passed through the slab. However, many factor—such as the amount of required conductivity (resistivity) for the optimized amount of power consumption—still need investigation. Also, the impact of curing age on the long-term conductivity of ECC should be considered. Finally, the long-term durability of ECC slabs under electric shock and imposed thermal gradients deserves long-term monitoring.

To address some of these knowledge gaps, in this project, a microwave unit was set up and calibrated with reference materials to measure the permittivity of electrically conductive cementitious materials for self-sensing applications at various curing ages. The details of the calibration process and the post-processing method used to obtain permittivity from the measured S-parameters measured with the Nicholson-Ross-Weir (NRW) conversion method are discussed in this report.

Tests of the method on cement pastes with various water-to-cement ratios showed that the permittivity measurements were sensitive to the water content and water consumption by the cement hydration and the development of a microstructure over the 28-day curing period. Curing age had a significant impact on the electrical conductivity of ECC. Chopped carbon fibers were found to be effective at increasing the permittivity and electrical conductivity of plain cement

paste by a maximum of eight times. Added carbon fibers were found to increase the electrical conductivity up to a certain amount, indicating a percolation limit beyond which fibers become obstructive to the electric path.

Further optimization of carbon fibers in heating-cooling simulations will be required to achieve maximum thermal-electrical efficiency with minimum power consumption. The durability of ECC under high current and thermal gradients also needs long-term monitoring. Finally, the recycling of abundant waste for the production of ECC should be evaluated.

CHAPTER 1. Overview

Road users' winter safety and mobility depend on effective winter road maintenance operations that promptly make winter road surface conditions safe. Current ice and snow control operations involve substantial applications of various kinds of deicers, which have undesirable implications for natural and built environments. Environmentally friendly winter maintenance solutions are needed to achieve required safety and mobility levels while also minimizing deicer agents' harmful effects on the environment. Research has shown that with recent advances in composite materials technology and manufacturing, it is possible to develop conductive pavement materials that offer ice and snow-melting capabilities to potentially decrease chemical deicer applications.

Research has shown that various methods could be used to heat the pavement surface for deicing without the application of deicers. Recently, research has focused on electrically conductive pavement materials that self-heat under a passing electric current. Consequently, this study's focus was to preliminarily explore possible additives that would increase the conductivity of pavement materials as a snow and ice control solution that could replace the use of sanding, deicing, and anti-icing on the roads.

In the first stage of the study, researchers evaluated the utility of commonly used nondestructive resistivity methods that have recently become prevalent for evaluating the microstructure and durability of concrete based on concrete resistivity. After the initial evaluation of these methods, the researchers identified the need for a different method of measurement that would be sensitive to the evolving microstructure of the cement and fiber/nanofiber additions at the desired frequency. On the basis of a review of the literature (Bois, Benally, and Zoughi, 2001; Donnell *et al.*, 2013; Donnell, Zoughi and Kurtis, 2013) and

communication with experts, a microwave method that uses a waveguide analyzer in the S-band frequency range was determined to be sensitive and effective at detecting the microstructure characteristics of the cement.

After calibration and validation, a microwave method based on dielectric spectroscopy in the S-range was used to explore various conductive additions to the cement paste. Of the tested fibers/nanofibers (steel fibers, carbon fibers, and carbon nanotubes), the conductive elements that resulted in an electrically conductive concrete (ECC) were carbon fibers. Next, a concentration study was performed with the carbon fibers, which indicated a possible percolation limit in the range of 0.2 to 0.3 percentage by weight (wt%). However, improvements in the mechanical properties of concrete were not achieved with the use of carbon fibers.

Future investigation of this topic may include evaluating other conductive elements, such as recycled carbon fibers and recycled carbon fiber composites (CFRP), carbon black, and other sources, especially from unwanted and rapidly generated industrial wastes. also Also suggested for future investigation are simultaneous optimization of electrical, mechanical, and durability properties, and an environmental life cycle cost assessment of the impacts of ECC solutions on the environmental, societal, and economic aspects of self-melting pavements. Guidelines were also developed for the future study of the thermal-electrical efficiency of ECC with optimized conductive content.

CHAPTER 2. Electrically Conductive Pavement Materials for Self-Deicing

2.1. Literature Review

With the application of sodium chloride (NaCl) and other deicer agents (calcium chloride ($CaCl_2$) and magnesium chloride ($MgCl_2$)) on roads for ice and snow control, the concentrations of chloride complexes increase in water and soils, which may harm the environment (Bäckström *et al.*, 2004). Furthermore, deicer agents negatively affect the built environment by chemically reacting with concrete and developing damaging oxychloride formations (Monical *et al.*, 2016).

Therefore, lately, various smart road solutions have been explored and have shown promise to reduce the use of deicer chemicals. Most of these technologies are at the proof-of-concept and feasibility stages, and the long-term durability of these new road materials will require rigorous testing and development before they are ready for mainstream application. Furthermore, feasibility and implementation may be impeded by a combination of many factors, such as cost, availability, compatibility with existing road materials, power requirements, and the need to be considered in selection criteria.

One such road solutions dates to the early 2000s with the advent of electrically conductive concrete (ECC), which contains different types of conductive components that offer indoor radiant heating and outdoor snow-melting capabilities (Tumidajski *et al.*, 2003).

The incorporation of different fibers—i.e., carbon fiber, carbon nanotubes, steel fibers, brass fiber, and glass fiber—in asphalt and concrete pavements has become more versatile in the recent decade. These fibers are transcending concrete in terms of strength, ductility, self-healing, self-sensing, electrical conductivity, and more. Carbon fiber is one of the most frequently used types of fibers in high-strength concrete. In an early study, Chen and Chung (1993) demonstrated that carbon fibers increase the electrical conductivity of concrete, and this property can be

correlated with other properties such as self-healing, porosity, and more. The filaments in carbon fiber have a high tensile strength that ranges from 4 to 6 GPa (Jeon *et al.*, 2013). Carbon fiber production has increased, making it cost effective, especially if it is acquired as an industry by-product (Nguyen *et al.*, 2016). Carbon fiber disperses within the cement matrix, and the resulting microstructure produces a higher modulus of toughness of the cement-based material (Chen *et al.*, 2018). Han *et al.* (2016) also analyzed 6-mm-long carbon fibers in a cement matrix, both macroscopically and microscopically, and found that the flexural and compressive strength increases by 15 percent and 18 percent, respectively.

Concrete is a good electrical insulator, which means that it does not transport electrons, but the added fibers (i.e., steel fiber, carbon fiber) have been shown to impart a significant decrease in concrete's resistivity. When the fibers come in contact with the water inside the pores of the concrete, the free electrons in the fibers work like a conductive medium that transports the electrons, and that enables the cement matrix to transport electricity (Whittington, McCarter and Forde, 1981; Chiarello and Zinno, 2005; Berrocal *et al.*, 2018).

Xie, Gu and Beaudoin (1996) developed a concept called the threshold of percolation. Fiber percolation can ensure high electrical conductivity. It means that the volume fraction of fibers inside the cementitious material should be equal to or greater than the volume of the fibers' interconnected paths. Also, there is a critical fiber volume fraction range after which the electrical conductivity increases rapidly, known as the percolation transition zone (Xie, Gu and Beaudoin, 1996). This concept is crucial for deducing the optimum fiber content. Because using excessive fiber content produces no benefit in terms of conductivity or mechanical properties. In fact, with increasing fiber concentrations, the electrical conductivity of the cement matrix decreases. When the percolation zone is exceeded, the conductivity decreases, but before the

percolation zone is achieved, the cement matrix exhibits higher electric conductivity with increasing fiber amounts. Chiarello and Zinno (2005) also studied the contribution of the shape of the carbon fiber. The authors suggested that a higher aspect ratio of carbon fiber can lead to better conductive performance with the same fiber volume. In the literature, 6-mm and 10-mm-long carbon fibers have been favored for better electricity transition (Al-Dahawi *et al.*, 2016; Donnini, Bellezze and Corinaldesi, 2018).

Sassani, Arabzadeh, *et al.* (2018a) determined the carbon fiber percolation limit in cementitious material and the optimum amount of carbon fiber to obtain maximum conductivity (figure 2-1). They determined the percolation transition zone of carbon fiber to be 0.25 to 1 percent volume for paste, 0.6 to 1 percent volume for mortar, and 0.5 to 0.75 percent volume for concrete. The optimum fiber dosage for electrical conductivity for cement paste and mortar was assumed to be equal to 1 percent. Their study included testing at 28 days and 460 days to assess the electrical conductivity of reinforced concrete at a late age. At 28 days the conductivity of concrete was found to be 1.86×10^{-2} S/cm, and at 460 days it was 1.22×10^{-2} S/cm.

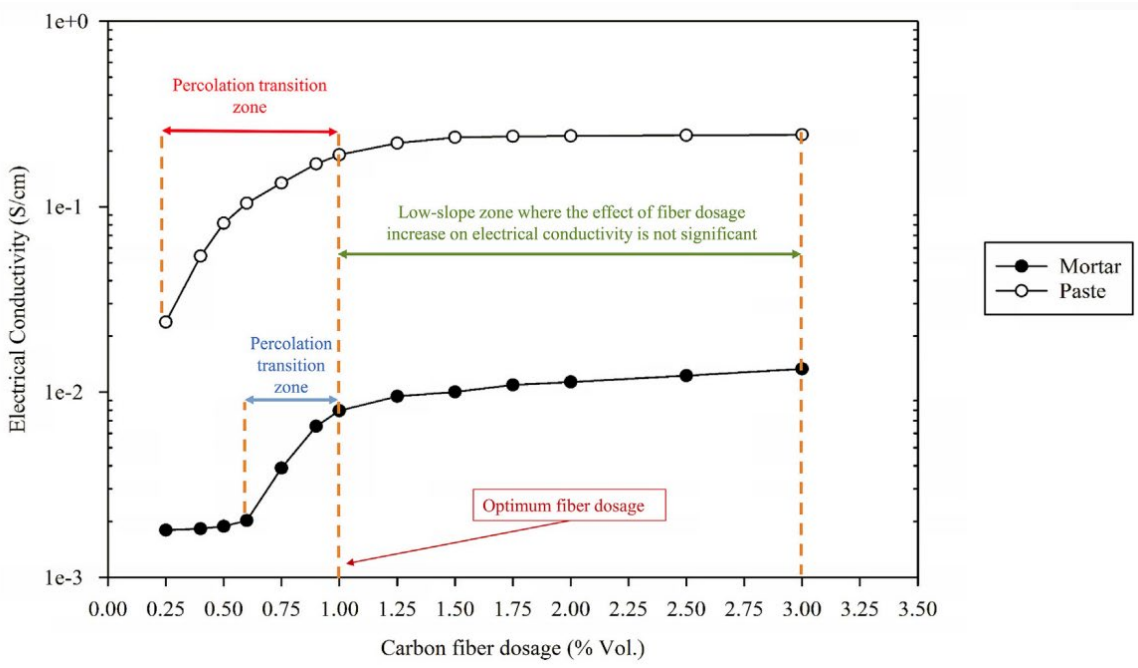

Figure 2-1: Snapshot of the fiber percolation zone for cement paste and mortar (from Sassani, Arabzadeh, *et al.*, 2018a)

Belli *et al.* (2020) studied the effects of three fibers and their percolation limits (figure 2-2), i.e., virgin carbon fiber (VCFs), recycled carbon fiber (RCF), and brass plated steel fiber. The authors compared all three fibers within a broad dosage range of 0.05 to 1.6 percent volume. The RCFs reduced conductivity by one order of magnitude but increased tensile and compressive strength by 100 percent. A feasibility study by Chang *et al.* (2009) showed that carbon nanofibers could be used as heating elements in concrete to offer ice-melting capabilities. Zhao *et al.* (2010) used carbon fiber wires in concrete slabs and showed that their electrothermal method effectively reduced snow.

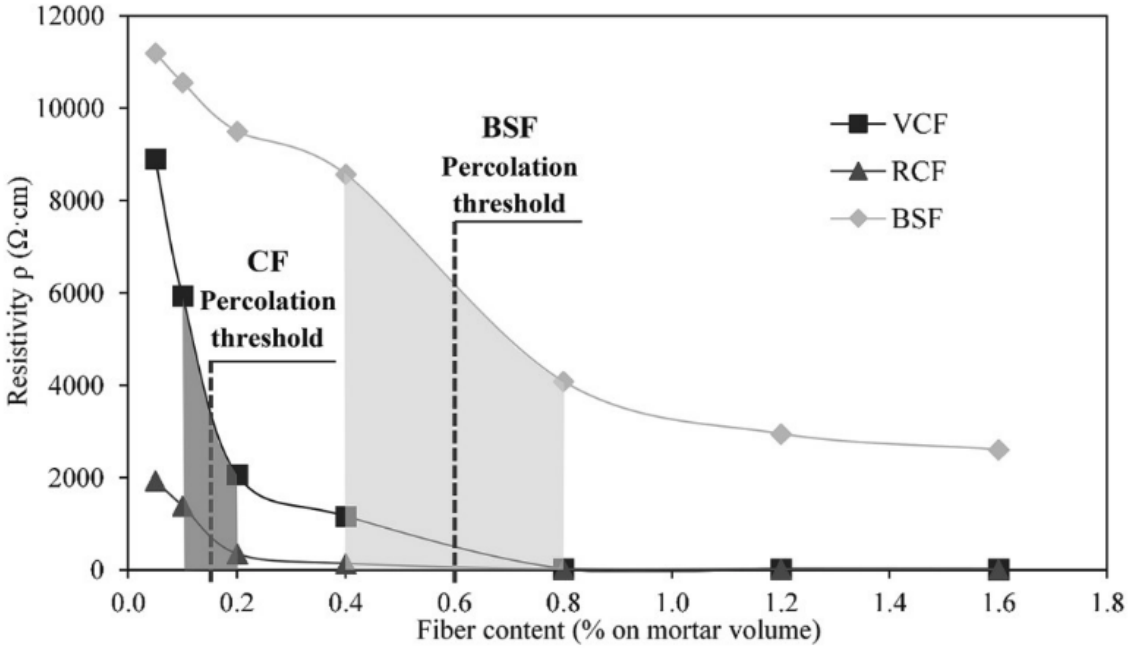

Figure 2-2: Snapshot of fiber percolation limit versus resistivity (Belli *et al.*, 2020).

Advancement in the nanotechnology field has also given rise to the use of carbon nanotubes (CNTs), nano-silica, nano-titanium dioxide, nano-iron oxide, nano-aluminum oxide,

and more., in pavement materials. Plain concrete is a brittle material, and under loading, it forms microcracks that lead to the ultimate failure of the structure if it is not repaired in time. The nanomaterials support the cement matrix, inhibit the propagation of microcracking, enhance durability, and provide good thermal conductivity (Liew, Kai and Zhang, 2016). CNT is a tube-shaped material resembling a rolled atom sheet (Iijima, 1991). CNTs are available in either single-walled (SWCNT) or multi-walled (MWCNT) kinds (Bethune *et al.*, 1993). The diameter and length of SWCNTs range, respectively, from 0.4 to 3 nm and 1 to 50 μm. For MWCNT, the width range is 1.4 to 100 nm, and the length varies from 0.1 to 100 μm (Chan and Andrawes, 2010; Materazzi, Ubertini and D'Alessandro, 2013; Han *et al.*, 2015).

The tensile strength for MWCNT ranges from 10 to 63 GPa, while for SWCNT, it can be as high as 600 GPa (Yu *et al.*, 2000; Zhao *et al.*, 2011). CNT has higher electrical conductivity than metals (Li, Wang and Zhao, 2005). SWCNT has shown higher electrical conductivity than MWCNT. MWCNT has a conductivity of 10^3 to 10^5 S/m (Siemens/meter), and SWCNT can exceed a conductivity of 10^6 S/m (Ahmad and Pan, 2009; Kumari *et al.*, 2009). Cement composite material has a very low electrical conductivity. The range is 10^{-6} to 10^{-9} S/cm. But the incorporation of CNT in the cement matrix increases the electrical conductivity as well as piezoresistivity. (Piezoresistivity means the change in electrical resistance under mechanical strain (Vossoughi, 2004)). Han *et al.* (2011) studied the piezoelectric response of CNT in cement composite with different load amplitudes. They found a linear correlation between the electrical resistivity and applied load within the elastic range, thus ensuring the sensing behavior of the concrete or cement composite materials with CNT. Kim *et al.* (2017) reported that 0.5 wt% of cement enhanced the electrical conductivity by 10^6 times. Singh *et al.* (2013) reported that 1.0

wt% of CNT increased the conductivity of cement paste to 10 S/cm. Coppola, Buoso and Corazza (2011) also reported a drastic change in electrical conductivity to almost 10 S/cm.

Carbon-based nanomaterials have demonstrated good mechanical and electrical performance for cement-based composite materials. However, they also have some drawbacks, especially because the dispersion of carbon-based nanomaterials is difficult (Dong *et al.*, 2016). Incorporating carbon fiber might increase the cement's electrical property, but durability is still questionable, especially homogeneity and the long-term performance of cement composite. Sonification or a dispersing reagent can be used to overcome the poor dispersion of CNTs (Han *et al.*, 2015). Steel fibers have good dispersion ability and can create a conductive network that can ensure the homogeneity of the introduced fiber through the samples (Dong *et al.*, 2016). Banthia, Djeridane and Pigeon (1992) found that the conductivity of cement mortar increases with the incorporation of 25 μm and 3-mm-lengths of steel fiber. Han *et al.* (2014) also showed that 0.36 percent of steel fiber resulted in a resistivity of 57 Ωcm (1.8×10^{-2} S/cm) and 0.72 percent volume produced a resistivity of 16 Ωcm (6.3×10^{-2} S/cm). Their steel fibers had a diameter of 8 μm. In a case study by Yehia *et al.* (2000), steel fibers used in concrete bridge decks showed promise for reducing snow and ice accumulation. The cost of the operation was estimated to be \$0.8/m^2 for the steel-reinforced concrete overlay per snowstorm.

Much of the literature on ECC and fiber-reinforced conductive concrete has focused on resistivity and conductivity performance, resistance change, electric heating, cooling law, and snow melting power, which is essential. But there is still a need to study the long-term durability of concrete under electric shock (high voltage has been used in most studies) and under thermal gradients. The impacts of curing age, microstructure, degree of hydration, and mixture composition of the ECC on its electrical-thermal performance also merit more investigation.

2.2. Research Objectives

The objective of this research was to develop a method of measurement able to accurately quantify the electrical properties of curing ECC as a function of curing age. Another objective was to create a prototype of at least one ECC with better conductivity than plain pavement materials. The electrical properties of the prototype ECC were quantified by using a microwave-based method over time. This report also presents a theoretical framework and guidelines for optimizing ECC conductivity while minimizing power consumption through heating-cooling simulation.

CHAPTER 3. Research Approach

3.1. Overview of Test Methods

Nondestructive testing (NDT) methods for construction materials are gaining popularity. Nondestructive testing is easy, cheap, accurte, and convenient in regard to time and labor intensity. Research on the use of NDT methods based on electromagnetic waves is increasing because of their unique ability to estimate the sustainability and durability of concrete. This method may be a preferred means for evaluating and monitoring concrete's structural health and the physical microstructure in comparison to other methods such as mercury intrusion porosimetry (MIP) (which can be destructive to the pore system), nuclear magnetic resonance (NMR) (which is costly to instrument), and others (Rajabipour and Weiss, 2007). Porosity, tortuosity, moisture content, corrosion susceptibility, and more, can be evaluated by measuring the conductivity of concrete (Gui, Qin and Li, 2016; Rangelov and Nassiri, 2018).

Quick and straightforward NDT methods of measuring the resistivity of concrete have recently gained popularity for evaluating durability (figure 3-1), but their application to a fiber-reinforced medium still requires investigation. In the initial phase of the study, surface resistivity and bulk resistivity measurements were evaluated for the purpose of developing an ECC based on a quick NDT method. However, these measurements did not yield expected trends with the addition of fibers. Therefore, a microwave method was developed, calibrated, and used to evaluate ECCs in this study.

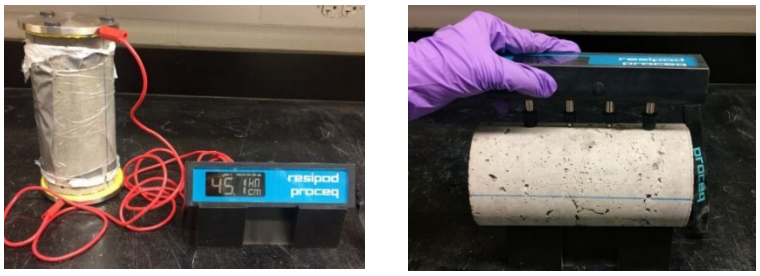

(a) (b)

Figure 3-1: (a) Bulk electrical resistivity meter, (b) surface resistivity meter measurement taken on a steel fiber reinforced concrete cylinder

Dielectric spectroscopy is pertinent in material sciences, communications, soil sciences, and biology (Ghodgaonkar, Varadan and Varadan, 1990; Gabriel, Lau and Gabriel, 1996; Raymond *et al.*, 2013). In this method, concrete is considered to be a dielectric material because of the pore solution. It is polarized in an electrical field. In the electrical field, the molecules inside the concrete reorient themselves to the applied field, which causes collisions and internal friction (Afsar *et al.*, 1986). The time it takes the molecules inside to reorient can be defined as relaxation time. The permittivity denotes this polarization. This value of permittivity has two parts: one is the real part, which is the dielectric constant, and the second part is imaginary, which is related to dielectric loss ($\varepsilon = \varepsilon' - i\varepsilon''$). The dielectric constant is the energy stored with exposure to the external electrical field. The dielectric property, also referred to as permittivity, measured as a function of frequency, is referred to as dielectric spectroscopy. The imaginary part is also referred to as a loss factor. The loss tangent or loss factor is the ratio of the imaginary part to the real part of the dielectric constant and represents the potential to dissipate microwave energy (Griffiths and Inglefield, 2005; Yaw (Rohde&Schwarz), 2006).

The measurement methods for the dielectric constant can be categorized into the transmission/reflection (T/R) method, open-ended coaxial probe method, open space method, and the resonant method. Among them, the T/R method is easy and widely used (Baker-Jarvis,

Vanzura and Kissick, 1990). In this method, the material under testing (MUT) is placed in a coaxial line or a waveguide while two ports in a vector network analyzer (VNA) measures the scattering parameters. This method was the preferred method in the present study. Necessary calibration should be carried out before measurement on the MUT is started. The calibration must be performed so that the reference plane of measurement is as close as possible to the MUT. The reflected scattering parameter (S11 or S22) and transmitted signal scattering parameters (S21 or S12) create a stiffness matrix for permittivity or permeability. These S-parameters need relevant post-processing to produce the complex dielectric value, as mentioned above. The Nicholson-Ross-Weir (NRW) model is a mathematical model that converts these four parameters (S11, S12, S21, S22) or just one pair (S11, S21) into both permittivity and permeability. Because of phase ambiguity, short samples are preferable for this conversion method. Otherwise, errors in the result are expected. However, it has not been determined how small the material should be (Nicolson and Ross, 1970).

For mechanical properties, the compressive strength (figure 3-2A) and flexural strength (figure 3-2B) of carbon fiber and steel fiber reinforced concrete mixes were characterized.

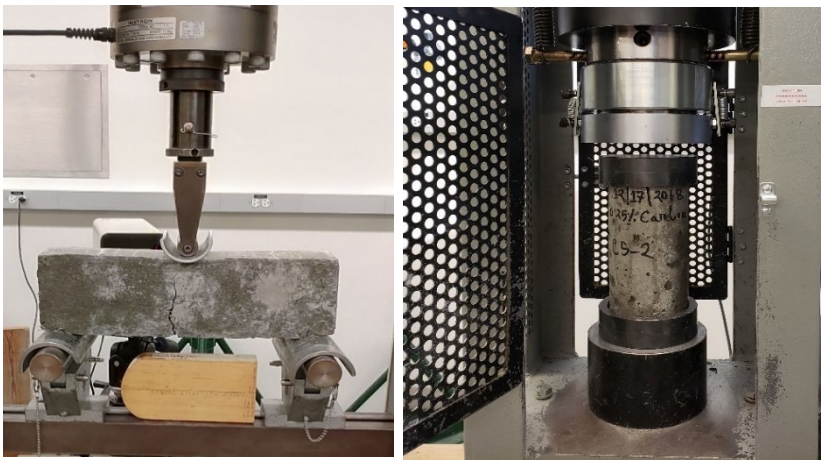

Figure 3-2: (A) flexural strength testing, (B) compressive strength

3.2. Microwave Method Set-up

A two-port vector network analyzer (VNA), PicoVNA™ 106 (figure 3-3a&b), was used for this study's experiments. This VNA operated between 300 kHz and 6 GHz. Two coaxial cables from the two ports were connected to the VNA, as shown in figure 3-3b. The other ends of the coaxial cables were connected with a coaxial to waveguide adapter. The rectangular waveguide adapter's frequency range was 2.60 to 3.95 GHz (S-Band waveguide adapter), which was within the operating range of the VNA. The inside dimensions of the adapter were 72.14 mm × 34.04 mm. The insertion loss of the waveguide was 0.2dB, which was low.

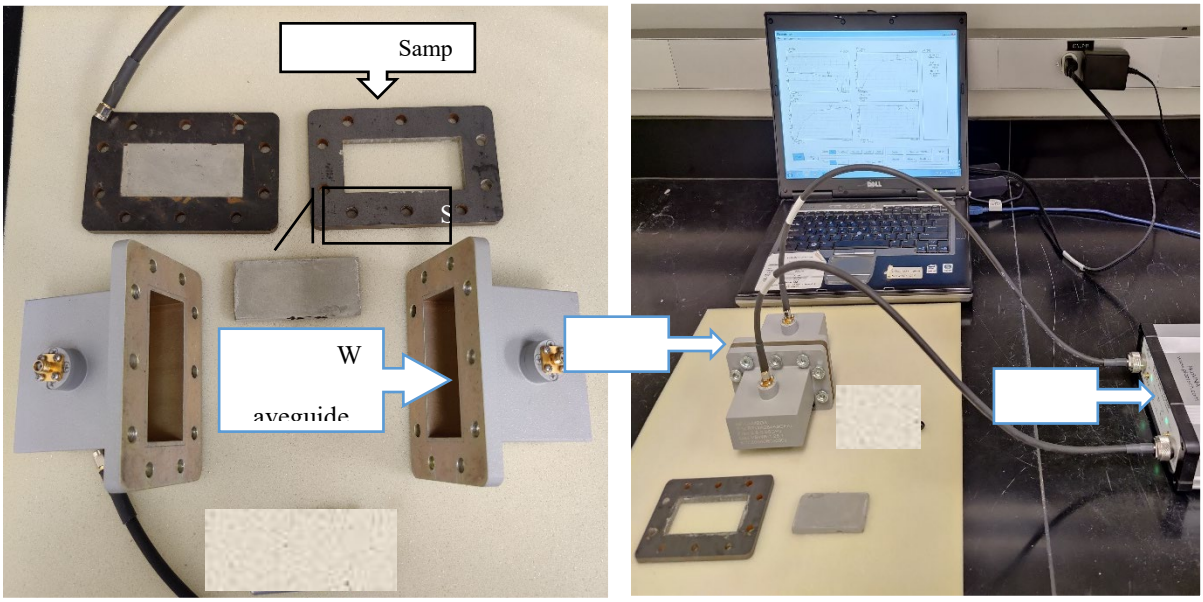

(a) (b)

Figure 3-3: (a) Waveguide adapter, sample holder, cement paste sample, and calibration tool, (b) The MUT (material under test) connected to a computer for S-parameter collection.

Before using the set-up on materials with an unknown permittivity, the VNA/waveguide set-up needed to be calibrated because the VNA measured the S-parameters via the initial port of the VNA. It did not consider the coaxial cable length and the waveguide. The measurement plane

needed to be transferred to the end of the waveguide adapter. Through-reflect-line (TRL) calibration was a two-port calibration better suited for the two-port VNA set-up.

The inside dimensions of the sample holder were the same as the waveguide adapter (72.14 mm × 34.04 mm). Several sample holders were machine shopped from steel and used as the mold to cast the cement samples. That way, a perfect cement fit was achieved inside the sample holder. The sample thickness was selected to be 6.35mm (1/4 inch) to avoid phase ambiguity. The VNA was additionally connected to a computer by USB cable, and the PicoVNA™ 2 software transfered the S-parameter readings, which were post-processed by the NRW method discussed above. A MATLAB program and a companion spreadsheet were developed to efficiently convert S-parameter readings into complex permittivity.

3.3. System Calibration by the TRL Method

Engen and Hoer (1979) first proposed the system error model (TRL calibration procedure). This error model was then simplified into a 12-term TRL calibration (*Network Analyzer Error Models and Calibration Methods* | www.rfmentor.com, no date). This calibration would allow us to measure only the MUT (material under testing) and remove the effects of the coaxial cables and adapter in the measurements. For thru measurement, the waveguide adapter ports were connected, and for the line, the sample holder was inserted between the two waveguide ports. A highly reflective metal disc was used as a short to measure the reflection. This was a two-term measurement in which S11 will S22 were used. The S11 was obtained when port 1 was connected to the short and S22 was obtained when port 2 was connected to the short.

TRL calibration started by converting the S-parameters of the thru measurement and delay lines to the T-parameter by using the following equations:

$$T = \begin{vmatrix} \frac{S_{11}S_{22}-S_{12}S_{21}}{S_{21}} & \frac{S_{11}}{S_{21}} \\ -\frac{S_{22}}{S_{21}} & \frac{1}{S_{21}} \end{vmatrix} \quad (3.3.1)$$

For the thru measurements, the S parameters are designated by S_t, the delay lines are S_d, and the converted T-parameter is T_t and T_d.

The variable T_v is represented as the product of T_d and $(T_t)^{-1}$.

$$T_v = T_d(T_t)^{-1} = \begin{vmatrix} t_{11} & t_{12} \\ t_{21} & t_{22} \end{vmatrix} \quad (3.3.2)$$

Using these four matrix elements, the following equation can be formed:

$$t_{21}x^2 + (t_{22} - t_{11})x - t_{12} = 0 \quad (3.3.3)$$

The two distinct roots are *b* and *(a/c).* One will be chosen in a way in which e_d<1 is the transmission coefficient of the delay line. By doing this, it is assumed that the delay line will be subjected to phase angle change close to 90 degrees, where e_d is expressed as

$$e_d = i\sqrt{-\frac{t_{12}(a/c)^{-1}+t_{11}}{t_{21}b+t_{22}}} \quad (3.3.4)$$

The S-parameters of the thru measurement are used for the next calculations,

$$d = -(S_{11}S_{22} - S_{12}S_{21}) \quad (3.3.5)$$

$$e = S_{11} \quad (3.3.6)$$

$$f = -S_{22} \quad (3.3.7)$$

$$g = S_{21} \quad (3.3.8)$$

Using *d*, *e*, *f*, *g* the next set of parameters are defined as follows:

$$\gamma = \frac{f-d(a/c)^{-1}}{1-e(a/c)^{-1}} \quad (3.3.9)$$

$$\left(\frac{\beta}{\alpha}\right) = \frac{e-b}{d-bf} \quad (3.3.10)$$

$$(a\alpha) = \frac{d-bf}{1-e(a/c)^{-1}} \quad (3.3.11)$$

The two reflect measurements Γ_1(Port 1 Short) and Γ_2(Port 2 Short) define the next parameter *(a/α),*

$$\left(\frac{a}{\alpha}\right) = \frac{(\Gamma_1 - b)(1+\Gamma_2\left(\frac{\beta}{\alpha}\right))}{(\Gamma_2+\gamma)(1-\Gamma_1\left(\frac{a}{c}\right)^{-1})} \tag{3.3.12}$$

Parameter *a* has two possible values, and one is chosen when Γ is close to $\Gamma_{estimate}$ where,

$$a = \pm\sqrt{(a\alpha)\left(\frac{a}{\alpha}\right)} \tag{3.3.13}$$

$$\Gamma = \frac{\Gamma_1 - b}{a - c\Gamma_1} \tag{3.3.14}$$

$$\Gamma_{estimate} = -e^{i/kl} \tag{3.3.15}$$

where *k* is the phase propagation constant and *l* is the length of the sample holder. The final calculation parameters are defined as,

$$\alpha = \frac{d - bf}{a(1 - e(a/c)^{-1})} \tag{3.3.16}$$

$$\beta = \alpha\left(\frac{\beta}{\alpha}\right) \tag{3.3.17}$$

$$k = \frac{g}{\alpha - f\beta} \tag{3.3.18}$$

$$c = a(a/c)^{-1} \tag{3.3.19}$$

This final set of parameters is used to define the calibration matrix variables:

$$T_1 = \begin{vmatrix} a & 0 \\ 0 & k\alpha \end{vmatrix} \tag{3.3.20}$$

$$T_2 = \begin{vmatrix} b & 0 \\ 0 & -k\gamma \end{vmatrix} \tag{3.3.21}$$

$$T_3 = \begin{vmatrix} c & 0 \\ 0 & -k\beta \end{vmatrix} \tag{3.3.22}$$

$$T_4 = \begin{vmatrix} 1 & 0 \\ 0 & k \end{vmatrix} \tag{3.3.23}$$

The uncalibrated S-parameters (S_u) obtained directly from the VNA are converted to actual S-parameters (S) by the following equations, and the reference plane is then transferred to the end of the waveguide adapter.

$$S = (T_1 - S_u T_3)^{-1}(S_u T_4 - T_2) \tag{3.3.24}$$

3.4. Conversion of S-Parameters to Dielectric Constant

As mentioned earlier, the Nicholson-Ross-Weir (NRW) conversion was used here to calculate the dielectric constant from the scattering parameter (S_{11}, S_{21}). S_{11}, S_{21} was the calibrated scattering parameter obtained from TRL calibration. The reflection coefficient can be presented as

$$\Gamma = X \pm \sqrt{X^2 - 1} \tag{3.4.1}$$

where $|\Gamma| < 1$ is required, and X in terms of s-parameter is defined as

$$X = \frac{S_{11}^2 - S_{21}^2 + 1}{2S_{11}} \tag{3.4.2}$$

The transmission coefficient T is defined as

$$T = \frac{S_{11} + S_{21} - \Gamma}{1 - (S_{11} + S_{21})\Gamma} \tag{3.4.3}$$

The permeability is given as

$$\mu_r = \frac{1+\Gamma}{\Lambda(1-\Gamma)\sqrt{\frac{1}{\lambda_0^2} - \frac{1}{\lambda_c^2}}} \tag{3.4.4}$$

Here, λ_0 and λ_c are the free-space wavelength and cutoff wavelength, respectively. For the S-band waveguide, the cutoff frequency is 14.42cm. Λ is defined as

$$\frac{1}{\Lambda^2} = -\left(\frac{1}{2\pi L} ln\left(\frac{1}{T}\right)\right)^2 \tag{3.4.5}$$

Here, L is sample thickness and real part of $1/\Lambda \geq 0$. Now, the permittivity is defined as

$$\varepsilon_r = \frac{\lambda_0^2}{\mu_r}\left(\frac{1}{\lambda_c^2} - \left[\frac{1}{2\pi L} ln\left(\frac{1}{T}\right)\right]^2\right) \tag{3.4.6}$$

This value of permittivity has two parts: one is the real part, which is the dielectric constant, and the second part is imaginary, which is related to dielectric loss ($\varepsilon = \varepsilon' - i\varepsilon''$).

The relationship between electrical conductivity (σ) and permittivity is expressed as

$$\sigma = \omega \varepsilon_0 \varepsilon' tan\phi \tag{3.4.7}$$

where ε_0 is the absolute dielectric permittivity, ω is the angular frequency, and $tan\phi$ is the ratio of imaginary and real parts of the dielectric permittivity.

CHAPTER 4. Materials

The dielectric constant and conductivity of neat cement paste (ordinary Portland cement + water) with different water-cement (w/c) ratios (0.35, 0.4, 0.5) over a 28-day curing period were characterized first. The sample holder from the waveguide set-up was used as the mold for casting the cement samples. During the casting of the cement samples, a glass plate was used as the base. The sample holder was taped to the glass plate with duct tape to avoid shifting during casting and finishing. After casting, the sample was sealed by placing another glass plate on top, so no water was lost to evaporation. The samples were kept inside the sample holder, inside double ziplock bags in sealed conditions, for the entire duration of testing. The sample was taken out every five days to take dielectric measurements and then was placed back into sealed conditions. A final measurement was taken after four months.

Next, different amounts of carbon nanotubes, carbon fibers, and steel fibers were added to one select cement paste composition with w/c=0.35. Carbon fibers were acquired from Toray, Inc. They had a filament diameter of 5 μm with a density of 1.81 g/cm^3. They had a tensile strength and tensile modulus of 5.5 GPa and 294 GPa, respectively. Their electric resistivity was 1.4×10^{-3} Ω-cm (figure 4-1).

PROPERTY	VALUE
CTE	-0.56 α ·10 $^{-6}$ /°C
Specific Heat	0.752 J/g ·°C
Thermal Conductivity	0.10 J/cm ·s·°C
Electric Resistivity	1.4 x 10^{-3} Ω·cm
Chemical Composition: Carbon	>96%
Na + K	<50 ppm

Figure 4-1: Snapshot of the functional properties of the carbon fibers from Toray Inc.

From the spool of carbon fiber, discrete pieces were cut in 10-mm lengths (figure 4-2). The cut carbon fibers were dispersed by manual mixing in water and then added to the cement paste and mixed again. The tested amounts were 0.2, 0.3, and 0.4 wt% of the dry cement.

Figure 4-2: Chopped up carbon fiber (10-mm length) for the experiment

Other tested fibers and nanofibers included carbon nanotubes and steel fibers. The mixing method for steel fibers was the same as that for the carbon fibers, and they were added in 1 percentage by weight concentrations. Steel fibers were cut in 10-mm-long pieces to fit inside the sample holder. The CNT size (inside diameter) was 1.3 to 50 nm, and the outside diameter was less than 5 nm. The length was 0.5 to 50 μm. The purity is above 90 percent, based on trace metal analysis.

Carbon nanotubes were tested in amounts of 0.05, 0.1, 0.2 wt% of dry cement. CNTs were added to water and sonicated for 10 minutes. Cement was then added to the CNT suspension and mixed manually.

CHAPTER 5. Results

5.1. Verification with Reference Materials

A set-up and calibration are valid when the experimental values for known materials are found and adhere to known values. Common materials used for validating a set-up are air, water, and wax (Kwon *et al.*, 2009; Hashemi *et al.*, 2015). In the current study, air and wax were used as reference materials. For validation, paraffin wax was melted and cast in the sample holder. After the paraffin had been set, the calibration procedure described in Section 3.3 was applied to the measurement set-up. Then measurements were taken with the empty sample holder (air as the sample) and the sample holder with the hard paraffin wax inside it. The calibrated values of the dielectric constant calculated by the NRW, as described previously, are presented in figure 5-1.

Figure 5-1: Dielectric constants of the reference materials over the waveguide frequency.

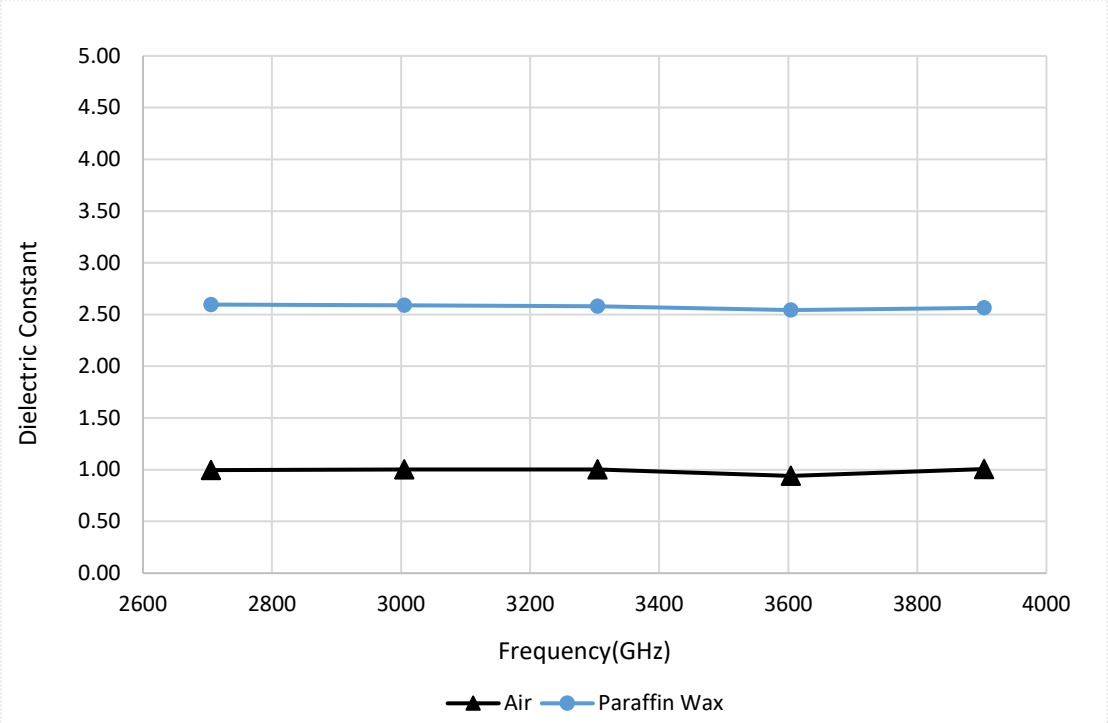

A value of 1 was obtained at all frequencies for the empty sample holder set-up, which agreed with the reported dielectric constant for air at close to 1 in the literature (Hector and

Schultz, 1936). Also, the dielectric constant for paraffin wax reported by Chakyar *et al*, (2017), was around 2.5 to 2.7 at room temperature, which agreed with the value of close to 2.5 seen in figure 5-1. Therefore, the calibration procedure was deemed suitable for continuing further experimentation with materials with an unknown dielectric constant.

5.2. Demonstration on Neat (No Fibers) Cement Paste

As mentioned above, three different water-cement ratios were selected for this experiment (0.35, 0.4, 0.5). Each sample's dimensions were 72.14×mm×34.04mm×6.35mm to fit exactly within the sample holder, as shown in figure 3-1. The samples were tested every five days over the S-band range, and the dielectric constant of about 3 GHz reported in figure 5-2 was a representative value.

Figure 5-2 shows that the dielectric constant one day after mixing was 29.1, 23.5, and 22.6 for the three mixes. These values had dropped to 13.5, 13.6, 13.8, respectively, at day 28. As the hydration progressed, the dielectric constant decreased. At about 14 days, the w/c ratios of 0.4 and 0.35 converged, indicating the decreasing amount of free water in the system. At day 28, the highest w/c ratio showed the lowest dielectric constant, albeit the measured values for all three mixes were very similar.

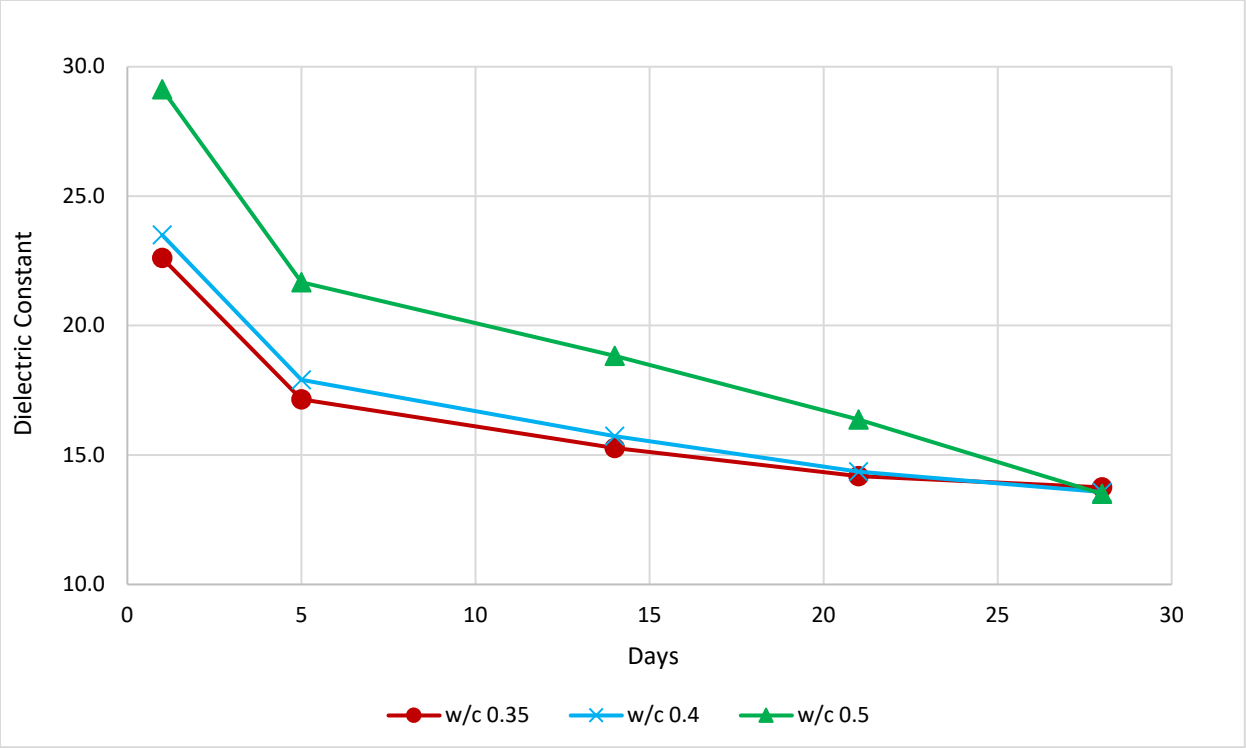

Figure 5-2: Changes in dielectric constants over time for cement pastes of different w/c ratios

After 28 days, the dielectric constant for the 0.5 w/c ratio was the lowest of the three, and that for the 0.35 w/c ratio was the highest. Though the dielectric constant was very close for all three mixes (13.5, 13.6, 13.8), the pattern logically followed the higher amount of capillary voids in mixes with a higher w/c ratio and thus the lowest dielectric value. Because the mixes with a w/c ratio of 0.5 had a higher amount of mixing water, there would be a higher porosity inside that sample, thereby resulting in a lower dielectric constant (Shalaby and Zoughi, 1995).

To better study late-age dielectric properties, the samples were kept in fully sealed conditions for another 90 days. Measurements were taken at four months on all three mixes. Figure 5-3 shows the dielectric constants reported after four months to study the inversion pattern. As mentioned earlier, the inversion started almost at 28 days, and it continued thereafter. After 90 days the pattern was clearly visible. The mix with a w/c ratio of 0.35 had the higher

dielectric constant at around 9.5, and the mix with a w/c ratio of 0.5 had the lowest, which was close to 7.5 (figure 5-3).

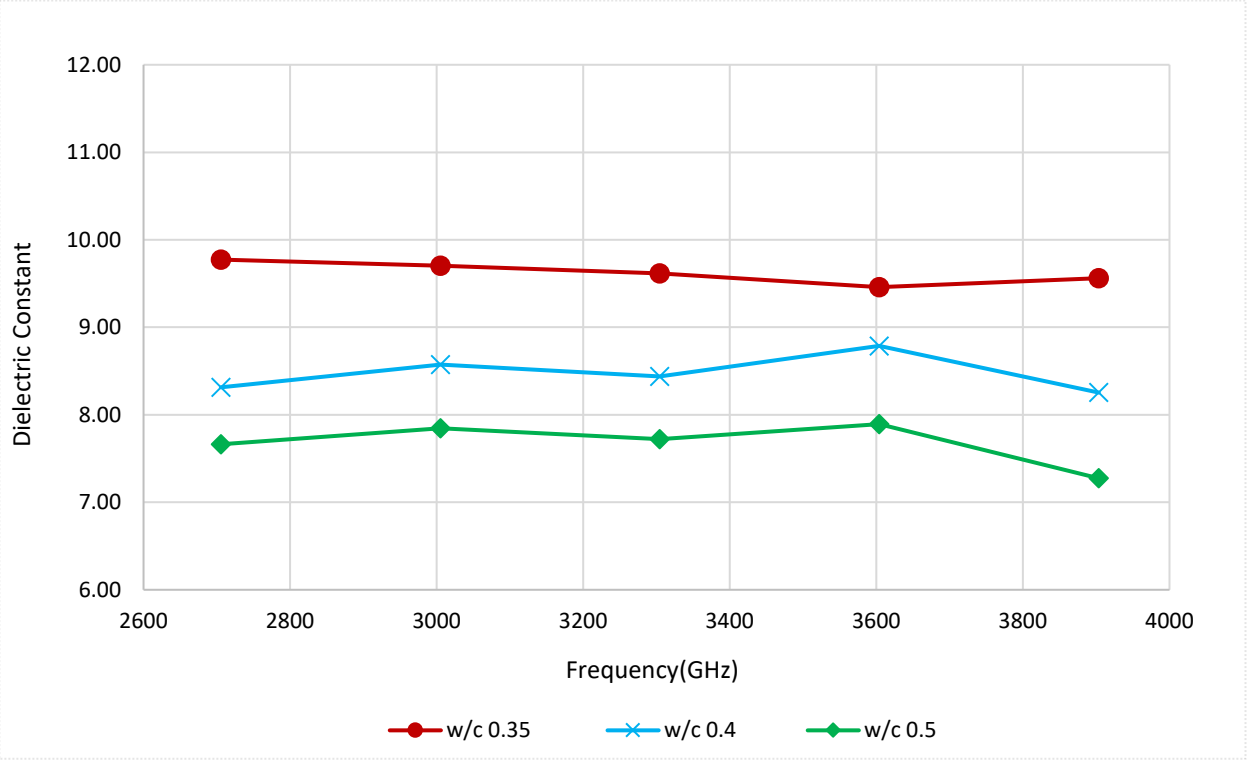

Figure 5-3: Dielectric constants of different w/c ratios at four months

These experiments with measurements of plain cement paste with various w/c ratios showed that the developed and calibrated system was sensitive to changes in cement paste microstructure and pore solution content and also to changes in the microstructure with curing age.

5.3. Cement Paste (w/c=0.35) with Carbon Fiber Additions

Figure 5-4 shows the measured dielectric constant for the cement paste with chopped carbon fibers added at 0.2, 0.3, and 0.4 percentage by weight . For every mix, one sample was cast. According to figure 5-4, the carbon fiber additions resulted in a significant initial increase

in dielectric constant after 24 hours, which was almost 770 percent,467 percent, and 232 percent higher, respectively, than the control for 0.2, 0.3, and 0.4 wt%.

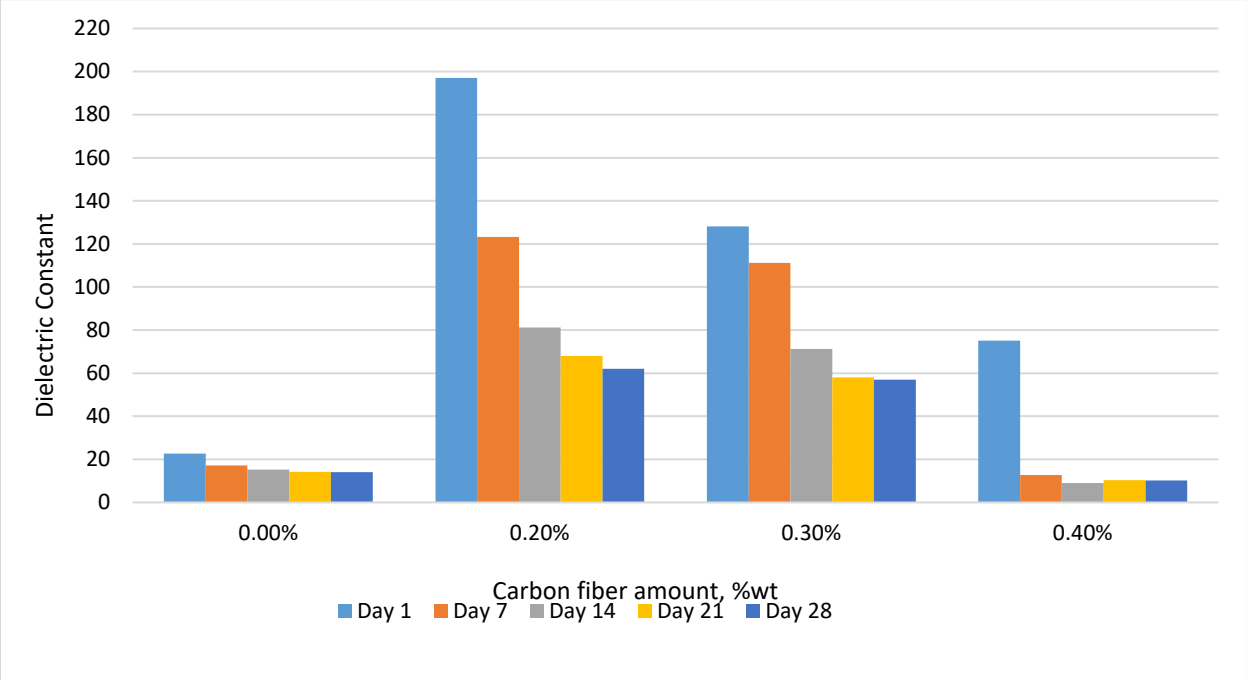

Figure 5-4: Changes in weekly dielectric constants for carbon fibers

All three mixes declined in dielectric values with age. A decline in the electrical properties of ECC with curing age wad also been reported in the literature (Sassani, Arabzadeh, *et al.*, 2018b), demonstrated by the microstructure of the matrix becoming more disconnected and the electrical path obstructed by hydration products.

For 0.2 wt% of carbon fiber, the 1-day dielectric constant was approximately 197, and after 28 days, it became 62. The third- and fourth-week data were similar, with hardly any change, meaning that hydration was almost complete. But the dielectric value was higher than the control because of the presence of carbon fiber. The reason for the instant boost could have been the filament distribution. The carbon fiber seemed to have created an interconnected network for transferring electrons. Figure 5-4 also shows that the percolation threshold for carbon fiber may have been within 0.2- to 0.3 wt%. After 0.3 wt% there was a decline in the

dielectric constant of 0.4 wt%, indicating that this amount may have passed beyond the percolation zone, as discussed previously (see the literature review, figures 2-1 and 2-2 (percolation zone 0.25 to 1 Vol%)). The authors suggested (see figure 2-2) that the percolation limit for carbon fiber was close to 0.2 wt%, which agreed with the findings of this study.

The dielectric constant of 0.4 wt% showed a significant decline to almost 13 in the second week, which was slightly lower than the control. The reason for this drop at day 7 was not clear, but perhaps with the high dosage, the carbon fiber stacked or clumped together, contributing to the lower dielectric constant.

Another way to observe and compare the relative changes due to the introduction of different fibers was to use the reflection coefficient, Γ. The reflection coefficient indicates how much electromagnetic wave is reflected because of the medium change in comparison to the incident wave (COSTA DP, 1970). The reflection coefficient is expressed by $\acute{R} = \Gamma e^{i\phi}$, which is a complex number, but the magnitude Γ represents the reflection coefficient value because the phase ϕ does not reveal much information.

An increase in the reflection coefficient indicates an increase in the water to cement ratio (Mubarak, Bois and Zoughi, 2001). Although we were not comparing different water to cement ratios, it was clear that a rise in a dielectric constant would also result in a rise in the reflection coefficient.

Figure 5-5 shows that the reflection coefficient of all carbon fiber mixes was higher than the control on day 28. The highest value was achieved with a 0.2 wt% carbon fiber, which was approximately 0.9, and the control value was 0.68. Carbon fibers at 0.3 wt% and 0.4 wt% also had higher values than the control but lower than 0.2 wt%, as those mixes were deemed to be beyond the percolation zone.

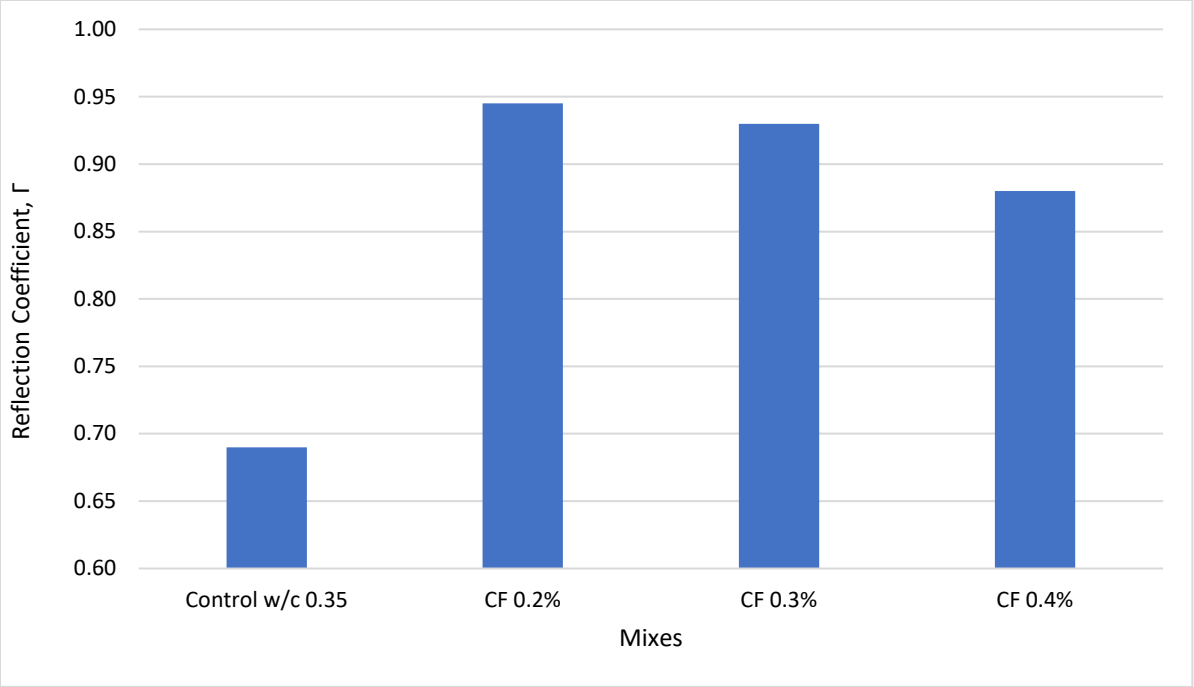

Figure 5-5: The reflection coefficients on day 28 for all mixes at around 3 GHz

To compare the electrical properties of the ECC developed in this study with those reported in the literature, the measured dielectric constant was theoretically converted to electrical conductivity by using Equation (3.4.7). As seen in table 5.1, the developed ECC in this study compared well with the average reported value developed by Sassani *et al* (2018*).* In their study, the w/c ratio was 0.42, which was slightly higher than that in this study (w/c 0.35). The carbon fiber dosages used in the study were 0.25 percentage by volume (vol%), 0.5 vol%, 0.75 vol%, etc., and the values shown in table 5. 1 were extrapolated to obtain amounts matching those used in this study.

Table 5. 1: Comparison of conductivity values from this study with those from the literature

Mixes	Conductivity (S/cm)	
	This study	ECC by (Sassani, Arabzadeh, *et al.*, 2018b)
0.2 wt% carbon fiber	4.57E-02	2.15E-02

0.3 wt% carbon fiber	3.61E-02	3.50E-02
Control	6.06E-03	9.15E-03

5.4. Cement Paste (w/c=0.35) with Other Types of Fibers

Steel fibers at 1 wt% and carbon nanotubes (CNTs) were also tested in the cement paste matrix. CNTs were added in the amounts of 0.05 wt%, 0.1 wt%, and 0.2 wt% of the dry cement. The dielectric constants were measured every 7 dasy until day 28 day for all three amounts in comparison to the control (neat paste). As seen in table 5-2, an ECC was not achieved by using the CNTs and the tested amounts of steel fibers. Different types and dosages of steel fibers and CNTs will be evaluated in future phases of the project to develop an ECC using these conductive additives.

Table 5. 2: Changes in weekly dielectric constants for various amounts of CNT

Day	Control W/C 0.35	CNT 0.05%	CNT 0.1%	CNT 0.2%	Steel 1%
Day 1	22	28	29	31	23
Day 7	18	19	20	19	20
Day 14	17	19	20	20	19
Day 21	17	17	18	19	18
Day 28	17	17	17	18	17

5.5. Mechanical Properties of Steel and Carbon Fiber Reinforced Mixes

Durability and mechanical performance are important requirements of ECC for pavement applications. Therefore, the compressive and flexural strengths of the mixes containing various amounts of steel fibers and carbon fibers were evaluated, and the results are presented in tables 5.3 and 5.4. Please note that mechanical testing was performed in the first stage of the study; therefore, the incorporated fiber ratios were different than those used in the ECC evaluation.

As seen in the tables, the additions of steel fibers in amounts higher than 0.25 percent increased the compressive and flexural strengths. Carbon fibers, on the other hand, resulted in a decline in mechanical properties in comparison to the neat mix. The carbon fiber length, mixing procedure, and dispersion influenced mechanical performance. Overall, all compressive strengths were above the 4500 psi required for highway paving, and flexural strength was higher than 650 psi. Furthermore, optimization of the size and amounts of carbon fibers was required to balance the electrical and mechanical performance of the ECC mixes.

Table 5. 3: 28-day compressive strengths of all mixes

Mix	Compressive Strength (psi)	STDV
Control	6,520	132
0.25% steel fiber	5,470	121
0.5% steel fiber	7,150	384
0.75% steel fiber	7,040	310
0.25% Carbon fiber	3,581	306
0.50% Carbon fiber	3,293	62
0.75% Carbon fiber	4,601	173

Table 5. 4: 28-day flexural strengths of all mixes

Mix	Modulus of Rupture (psi)	SDV
Control	797	33
0.25 % Steel	741	56
0.5 % Steel	850	12
0.75 % Steel	932	18
0.25 % Carbon	784	46
0.5 % Carbon	663	18
0.75 % Carbon	641	44

5.6. Theoretical Framework for Heating and Cooling Simulations

An electrothermal analysis was required to evaluate the efficiency of the ECC slabs at raising the concrete temperature for ice and snow removal while a current is passed through the slab. Based on the law of the conservation of energy, Equation 5.6.1 shows the rate of change in the stored energy in the control volume at any point in time,

$$\frac{d}{dx}\left(k.\frac{dT}{dx}\right) = \rho C_p \frac{dT}{dt} \tag{5.6.1}$$

In this equation, T is the slab nodal temperature, °C; t is time, and dt is the time increment, hours; ρ is the concrete's density, kg/m^3; Cp is the specific heat of the concrete, J/kg/°C; and finally, k is the thermal conductivity of the concrete, W/m/°C.

For heating, a constant voltage is applied to embedded electrodes within the slab. Current, I (A) and temperature T(°C) are recorded for a fixed monitoring period. The samples' electrical resistance R are estimated with the Ohm's and Joule's laws,

$$P = VI = \frac{V^2}{R} \tag{5.6.2}$$

where P (W) is the electric power as a function of the applied voltage V (V), current I (A).

Fitting a regression line through plots of P versus temperature rise gives the energy transfer coefficient, *h*, estimated for the ECC slab. Gomis *et al.* (2015) also reported the heat transfer parameter *hA* =0.536W/°C, which can be directly used in equations (5.6.3) and (5.6.4). This also represents the heat dissipation or transfer with increasing or decreasing temperature.

Gomis *et al.* (2015) developed closed-form solutions for Equation 5.6.1 for a heating experiment to simulate heating experiments based on measured current and temperature.

$$T = T_r + \frac{P}{hA}[1 - e^{-\frac{hA\delta t}{mC_p}}] \tag{5.6.3}$$

where T(°C) is the temperature of the sample, T_r(°C) is the room temperature, A(m^2) is the exposed surface of the tested area, δt is the difference in time(sec), Cp is heat capacity (j/kg°C), m (kg) is the weight of the specimen, and h (W/m^2°C) is the heat transfer coefficient.

Once the power has been switched off, the cooling cycle is also reported as,

$$T = T_r + (T_{off} - T_r)\, e^{-\frac{hA\delta t}{mC_p}} \tag{5.6.4}$$

Here, T_{off} is the sample temperature when the power is turned off.

The simulated heating and cooling experiments from Gomis *et al.* (2015) are shown in figure 5-6 as examples. This simulation was done for a typical sidewalk (3 ft×3 ft), and the applied voltage was 100V for a plain mix and mixes containing amounts of carbon fibers,

according to the study. All thermal and electrical properties were assumed on the basis of the reported values in Gomis *et al.*(2015).

As shown in figure 5-6, the control had a maximum temperature increase of only 1.3°C, whereas carbon fibers at 0.2 wt% and 0.3 wt% showed an increase of almost 4.7°C and 10°C, respectively.

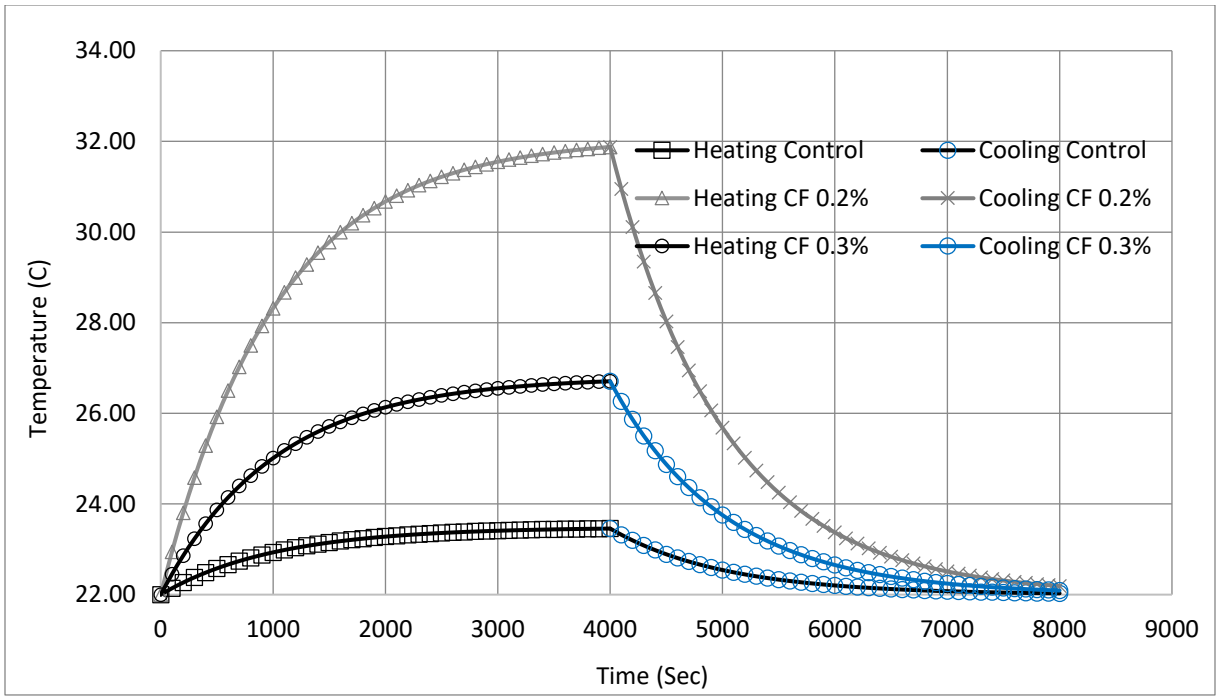

Figure 5-6: Temperature increase simulation for carbon fiber

CHAPTER 6. Conclusions

Record low temperatures, accompanied by ice and snow accumulation, were frequently experienced across the country this past winter. Adverse weather and road conditions disrupted businesses, flights, schools, and many other daily operations (*U.S. Feels Arctic Blast, Record Low Temperatures Nationwide*, no date*)*. Keeping up with winter conditions by extending hours of ice and snow control operations to clear the roads after frequent melt-freeze cycles and snowstorms burdens city and highway agencies with colossal operational, equipment, and labor costs (Nassiri, Bayat and Salimi, 2015). These operations include the application of salts, sand, and deicer chemicals on the road, which pollute the natural environment and harm fish and other aquatic species (Trombulak and Frissell, 2000). Also, salts and deicing chemicals are the most effective only within certain temperature ranges (typically above -10 deg C); equipment breakdowns in freezing conditions are another challenge associated with current winter maintenance operations (Sassani, Ceylan, *et al.*, 2018).

Studies have shown that ice and snow can be melted by passing an electric current through a concrete pavement slab that has been mixed with electrically conductive pavement materials. Carbon fibers have shown good potential for increasing the conductivity of concrete.

In this study, a method using microwaves was utlized to evaluate the conductivity of pavement materials that included fiber additions to improve snow and ice melting functionality. Dielectric constant measurements over the S-band frequency range were used to develop a prototype of an ECC with higher electrical conductivity than plain cement paste. The set-up used a relatively low-cost, small, and portable VNA and small samples for testing. After calibration, the measurement system showed great sensitivity to changes in the pore solution and microstructure of the cement during the curing period and to different water to cement ratios.

The required samples of cement for electrical testing were small, meaning that it is possible to sample in the field and laboratory and repeat the tests on several mixes and samples. The small sample sizes, nondestructive nature of the test, and quick measurements can be used to easily identify the optimum dosage and percolation limits of various conductive fibers for ECC development.

Of the tested conductive additives, carbon fibers seemed the most effective based on the experiments in this study. An ECC was developed in this study with 0.2 and 0.3 wt% carbon fibers that had 28-day resistivities of 22 Ω-cm and 28 Ω-cm, respectively. Testing the thermal and electrical properties as reported in the literature for similar ECC in a heating and cooling simulation showed that the developed ECC could raise the sample temperature by 4.7°C (0.2 wt% CF) and 9.9°C (0.3 wt% CF) degrees, respectively, under a 100V applied voltage.

Future investigations may include developing ECC mixes with green additives from recycled materials such as recycled carbon fibers and recycled carbon fiber-reinforced polymer. Also, it will be necessary to optimize the mix design to balance the trade-off between compressive strength and the required number of fibers for the required level of conductivity.

CHAPTER 7. References

Afsar, M. N. *et al.* (1986) 'The Measurement of the Properties of Materials', *Proceedings of the IEEE*, 74(1), pp. 183–199. doi: 10.1109/PROC.1986.13432.

Ahmad, K. and Pan, W. (2009) 'Dramatic effect of multiwalled carbon nanotubes on the electrical properties of alumina based ceramic nanocomposites', *Composites Science and Technology*. Elsevier, 69(7–8), pp. 1016–1021.

Al-Dahawi, A. *et al.* (2016) 'Effect of mixing methods on the electrical properties of cementitious composites incorporating different carbon-based materials', *Construction and Building Materials*, 104, pp. 160–168. doi: 10.1016/j.conbuildmat.2015.12.072.

Bäckström, M. *et al.* (2004) 'Mobilisation of heavy metals by deicing salts in a roadside environment', *Water Research*, 38(3), pp. 720–732. doi: 10.1016/j.watres.2003.11.006.

Baker-Jarvis, J., Vanzura, E. J. and Kissick, W. A. (1990) 'Improved technique for determining complex permittivity with the transmission/reflection method', *IEEE Transactions on Microwave Theory and Techniques*, 38(8), pp. 1096–1103. doi: 10.1109/22.57336.

Banthia, N., Djeridane, S. and Pigeon, M. (1992) 'Electrical resistivity of carbon and steel micro-fiber reinforced cements', *Cement and Concrete research*. Elsevier, 22(5), pp. 804–814.

Belli, A. *et al.* (2020) 'Commercial and recycled carbon/steel fibers for fiber-reinforced cement mortars with high electrical conductivity', *Cement and Concrete Composites*. Elsevier Ltd, 109(February), p. 103569. doi: 10.1016/j.cemconcomp.2020.103569.

Berrocal, C. G. *et al.* (2018) 'Electrical resistivity measurements in steel fibre reinforced cementitious materials', *Cement and Concrete Composites*, 89, pp. 216–229. doi: 10.1016/j.cemconcomp.2018.03.015.

Bethune, D. S. *et al.* (1993) 'Cobalt-catalysed growth of carbon nanotubes with single-atomic-layer walls', *Nature*. Springer, 363(6430), pp. 605–607.

Bois, K. J., Benally, A. D. and Zoughi, R. (2001) 'Near-field microwave non-invasive determination of NaCl in mortar', *IEE Proceedings: Science, Measurement and Technology*, 148(4), pp. 178–182. doi: 10.1049/ip-smt:20010482.

Chakyar, S. P. *et al.* (2017) 'Measurement of dielectric constant of waxes at different temperatures using split ring resonator structure', *2016 IEEE MTTS International Microwave and RF Conference, IMaRC 2016 - Proceedings*, 1(1), pp. 14–17. doi: 10.1109/IMaRC.2016.7939638.

Chan, L. Y. and Andrawes, B. (2010) 'Finite element analysis of carbon nanotube/cement composite with degraded bond strength', *Computational Materials Science*. Elsevier, 47(4), pp. 994–1004.

Chang, C. *et al.* (2009) 'A feasibility study of self-heating concrete utilizing carbon nanofiber heating elements', *Smart Materials and Structures*, 18(12). doi: 10.1088/0964-1726/18/12/127001.

Chen, P. W. and Chung, D. D. L. (1993) 'Carbon fiber reinforced concrete for smart structures capable of nondestructive flaw detection', *Smart Materials and Structures*, 2(1), pp. 22–30. doi: 10.1088/0964-1726/2/1/004.

Chen, Z. shun *et al.* (2018) 'Mechanical behavior of multilayer GO carbon-fiber cement composites', *Construction and Building Materials*. Elsevier Ltd, 159, pp. 205–212. doi: 10.1016/j.conbuildmat.2017.10.094.

Chiarello, M. and Zinno, R. (2005) 'Electrical conductivity of self-monitoring CFRC', *Cement and Concrete Composites*, 27(4), pp. 463–469. doi: 10.1016/j.cemconcomp.2004.09.001.

Coppola, L., Buoso, A. and Corazza, F. (2011) 'Electrical properties of carbon nanotubes cement composites for monitoring stress conditions in concrete structures', in *PROTECT 2011. Performance, Protection & Strenghtening of Structures under Extreme Loading. Third International Workshop.* Trans Tech Publications, pp. 118–123.

COSTA DP (1970) 'Transmission Line Fundamentals', *Instrum Contr Syst*, 43(4), pp. 101–102. doi: 10.1016/b978-0-12-418663-7.00001-0.

Dong, S. *et al.* (2016) 'Electrically conductive behaviors and mechanisms of short-cut super-fine stainless wire reinforced reactive powder concrete', *Cement and Concrete Composites*. Elsevier Ltd, 72, pp. 48–65. doi: 10.1016/j.cemconcomp.2016.05.022.

Donnell, K. M. *et al.* (2013) 'Wideband microwave characterization of alkali-silica reaction (ASR) gel in cement-based materials', *Materials Letters*. Elsevier, 90, pp. 159–161. doi: 10.1016/j.matlet.2012.09.017.

Donnell, K. M., Zoughi, R. and Kurtis, K. E. (2013) 'Demonstration of microwave method for detection of alkali-silica reaction (ASR) gel in cement-based materials', *Cement and Concrete Research*. Elsevier Ltd, 44, pp. 1–7. doi: 10.1016/j.cemconres.2012.10.005.

Donnini, J., Bellezze, T. and Corinaldesi, V. (2018) 'Mechanical, electrical and self-sensing properties of cementitious mortars containing short carbon fibers', *Journal of Building Engineering*. Elsevier Ltd, 20(April), pp. 8–14. doi: 10.1016/j.jobe.2018.06.011.

Engen, G. F. and Hoer, C. A. (1979) 'Thru-reflect-line: An improved technique for calibrating the dual six-port automatic network analyzer', *IEEE transactions on microwave theory and techniques*. IEEE, 27(12), pp. 987–993.

Gabriel, S., Lau, R. W. and Gabriel, C. (1996) 'The dielectric properties of biological tissues: II. Measurements in the frequency range 10 Hz to 20 GHz', *Physics in Medicine and Biology*, 41(11), pp. 2251–2269. doi: 10.1088/0031-9155/41/11/002.

Ghodgaonkar, D. K., Varadan, V. V. and Varadan, V. K. (1990) 'Free-Space Measurement of Complex Permittivity and Complex Permeability of Magnetic Materials at Microwave Frequencies', *IEEE Transactions on Instrumentation and Measurement*, 39(2), pp. 387–394. doi: 10.1109/19.52520.

Gomis, J. *et al.* (2015) 'Self-heating and deicing conductive cement . Experimental study and modeling', *Construction and Building Materials*. Elsevier Ltd, 75, pp. 442–449. doi: 10.1016/j.conbuildmat.2014.11.042.

Griffiths, D. J. and Inglefield, C. (2005) ' Introduction to Electrodynamics ', *American Journal of Physics*, 73(6), pp. 574–574. doi: 10.1119/1.4766311.

Gui, Q., Qin, M. and Li, K. (2016) 'Gas permeability and electrical conductivity of structural concretes: Impact of pore structure and pore saturation', *Cement and Concrete Research*, 89, pp. 109–119. doi: 10.1016/j.cemconres.2016.08.009.

Han, B. *et al.* (2011) 'Sensing properties of CNT-filled cement-based stress sensors', *Journal of Civil Structural Health Monitoring*. Springer, 1(1–2), pp. 17–24.

Han, B. *et al.* (2014) 'Nanotip-induced ultrahigh pressure-sensitive composites: principles, properties and applications', *Composites Part A: Applied Science and Manufacturing*. Elsevier, 59, pp. 105–114.

Han, B. *et al.* (2015) 'Review of nanocarbon-engineered multifunctional cementitious composites', *Composites Part A: Applied Science and Manufacturing*. Elsevier, 70, pp. 69–81.

Han, B. *et al.* (2016) 'Reinforcement effect and mechanism of carbon fibers to mechanical and electrically conductive properties of cement-based materials', *Construction and Building Materials*. Elsevier Ltd, 125, pp. 479–489. doi: 10.1016/j.conbuildmat.2016.08.063.

Hashemi, A. *et al.* (2015) 'Comparison of Alkali-Silica Reaction Gel Behavior in Mortar at Microwave Frequencies', *IEEE Transactions on Instrumentation and Measurement*. IEEE, 64(7), pp. 1907–1915. doi: 10.1109/TIM.2014.2367771.

Hector, L. G. and Schultz, H. L. (1936) 'The dielectric constant of air at radiofrequencies', *Journal of Applied Physics*, 7(4), pp. 133–136. doi: 10.1063/1.1745374.

Iijima, S. (1991) 'Helical microtubules of graphitic carbon', *Nature*, 354(6348), pp. 56–58. doi: 10.1038/354056a0.

Jeon, Y. P. *et al.* (2013) 'Carbon fibers', *Handbook of Advanced Ceramics-materials, Applications, Processing and Properties*. Elsevier Science Ltd, pp. 143–154.

Kim, G. M. *et al.* (2017) 'Electrical characteristics of hierarchical conductive pathways in cementitious composites incorporating CNT and carbon fiber', *Cement and Concrete Composites*. Elsevier Ltd, 82, pp. 165–175. doi: 10.1016/j.cemconcomp.2017.06.004.

Kumari, L. *et al.* (2009) 'Synthesis, microstructure and electrical conductivity of carbon nanotube–alumina nanocomposites', *Ceramics International*. Elsevier, 35(5), pp. 1775–1781.

Kwon, S.-J. *et al.* (2009) 'An Experimental Study on Evaluation of Compressive Strength in Cement Mortar Using Averaged Electromagnetic Properties', *International Journal of Concrete Structures and Materials*, 3(1), pp. 25–32. doi: 10.4334/ijcsm.2009.3.1.025.

Li, G. Y., Wang, P. M. and Zhao, X. (2005) 'Mechanical behavior and microstructure of cement composites incorporating surface-treated multiwalled carbon nanotubes', *Carbon*. Elsevier, 43(6), pp. 1239–1245.

Liew, K. M., Kai, M. F. and Zhang, L. W. (2016) 'Carbon nanotube reinforced cementitious composites: An overview', *Composites Part A: Applied Science and Manufacturing*. Elsevier Ltd, 91, pp. 301–323. doi: 10.1016/j.compositesa.2016.10.020.

Materazzi, A. L., Ubertini, F. and D'Alessandro, A. (2013) 'Carbon nanotube cement-based transducers for dynamic sensing of strain', *Cement and Concrete Composites*. Elsevier, 37, pp. 2–11.

Monical, J. *et al.* (2016) 'Reducing joint damage in concrete pavements: Quantifying calcium oxychloride formation', *Transportation Research Record*, 2577(2577), pp. 17–24. doi: 10.3141/2577-03.

Mubarak, K., Bois, K. J. and Zoughi, R. (2001) 'A simple, robust, and on-site microwave technique for determining water-to-cement ratio (w/c) of fresh Portland cement-based materials', *IEEE Transactions on Instrumentation and Measurement*, 50(5), pp. 1255–1263. doi: 10.1109/19.963194.

Nassiri, S., Bayat, A. and Salimi, S. (2015) 'Survey of practice and literature review on municipal road winter maintenance in Canada', *Journal of Cold Regions Engineering*, 29(3). doi: 10.1061/(ASCE)CR.1943-5495.0000082.

Network Analyzer Error Models and Calibration Methods | www.rfmentor.com (no date). Available at: https://www.rfmentor.com/content/network-analyzer-error-models-and-calibration-methods (Accessed: 14 April 2021).

Nguyen, H. *et al.* (2016) 'Cement mortar reinforced with reclaimed carbon fibres, CFRP waste or prepreg carbon waste', *Construction and Building Materials*. Elsevier Ltd, 126, pp. 321–331. doi: 10.1016/j.conbuildmat.2016.09.044.

Nicolson, A. M. and Ross, G. F. (1970) 'Measurement of the Intrinsic Properties Of Materials by Time-Domain Techniques', *IEEE Transactions on Instrumentation and Measurement*, 19(4), pp. 377–382. doi: 10.1109/TIM.1970.4313932.

Rajabipour, F. and Weiss, J. (2007) 'Electrical conductivity of drying cement paste', *Materials and Structures/Materiaux et Constructions*, 40(10), pp. 1143–1160. doi: 10.1617/s11527-006-9211-z.

Rangelov, M. and Nassiri, S. (2018) 'Empirical time-dependent tortuosity relations for hydrating mortar mixtures based on modified Archie's law', *Construction and Building Materials*, 171, pp. 825–838. doi: https://doi.org/10.1016/j.conbuildmat.2018.03.173.

Raymond, W. J. K. *et al.* (2013) 'Complex permittivity measurement using capacitance method from 300 kHz to 50 MHz', *Measurement: Journal of the International Measurement Confederation*. Elsevier Ltd, 46(10), pp. 3796–3801. doi: 10.1016/j.measurement.2013.06.039.

Sassani, A., Arabzadeh, A., *et al.* (2018a) 'Carbon fiber-based electrically conductive concrete for salt-free deicing of pavements', *Journal of Cleaner Production*. Elsevier Ltd, 203, pp. 799–809. doi: 10.1016/j.jclepro.2018.08.315.

Sassani, A., Arabzadeh, A., *et al.* (2018b) 'Carbon fiber-based electrically conductive concrete for salt-free deicing of pavements', *Journal of Cleaner Production*. Elsevier Ltd, 203, pp. 799–809. doi: 10.1016/j.jclepro.2018.08.315.

Sassani, A., Ceylan, H., *et al.* (2018) 'Development of Carbon Fiber-modified Electrically Conductive Concrete for Implementation in Des Moines International Airport', *Case Studies in Construction Materials*. Elsevier, 8, pp. 277–291. doi: 10.1016/J.CSCM.2018.02.003.

Shalaby, W. and Zoughi, R. (1995) 'Microwave Compressive Strength Estimation of Cement Paste Using Monopole Probes', *Research in Nondestructive Evaluation*, 7(2–3), pp. 101–115. doi: 10.1080/09349849509409571.

Singh, A. P. *et al.* (2013) 'Multiwalled carbon nanotube/cement composites with exceptional electromagnetic interference shielding properties', *Carbon*. Elsevier, 56, pp. 86–96.

Trombulak, S. C. and Frissell, C. A. (2000) 'Review of Ecological Effects of Roads on Terrestrial and Aquatic Communities', *Conservation Biology*. John Wiley & Sons, Ltd (10.1111), 14(1), pp. 18–30. doi: 10.1046/j.1523-1739.2000.99084.x.

Tumidajski, P. J. *et al.* (2003) 'Overlay current in a conductive concrete snow melting system', *Cement and Concrete Research*, 33(11), pp. 1807–1809. doi: 10.1016/S0008-8846(03)00198-4.

U.S. Feels Arctic Blast, Record Low Temperatures Nationwide (no date). Available at: https://www.thedailybeast.com/us-feels-arctic-blast-record-low-temperatures-nationwide (Accessed: 3 May 2021).

Vossoughi, F. (2004) 'Electrical Resistivity of Carbon Fiber Reinforced Concrete', *Carbon*.

Whittington, H. W., McCarter, J. and Forde, M. C. (1981) 'The conduction of electricity through concrete', *Magazine of concrete research*. Thomas Telford Ltd, 33(114), pp. 48–60.

Xie, P., Gu, P. and Beaudoin, J. J. (1996) 'Electrical percolation phenomena in cement composites containing conductive fibres', *Journal of Materials Science*. Springer, 31(15), pp. 4093–4097.

Yaw(Rohde&Schwarz), K. C. (2006) 'Measurement of dielectric material properties Application Note', *Measurement Techniques*, pp. 1–35.

Yehia, S. *et al.* (2000) 'Conductive concrete overlay for bridge deck deicing: mixture proportioning, optimization, and properties', *Materials Journal*, 97(2), pp. 172–181.

Yu, M.-F. *et al.* (2000) 'Strength and breaking mechanism of multiwalled carbon nanotubes under tensile load', *Science*. American Association for the Advancement of Science, 287(5453), pp. 637–640.

Zhao, H. M. *et al.* (2010) 'Concrete slab installed with carbon fiber heating wire for bridge deck deicing', *Journal of Transportation Engineering*, 136(6), pp. 500–509. doi: 10.1061/(ASCE)TE.1943-5436.0000117.

Zhao, J.-C. *et al.* (2011) 'Thermal conductive and electrical properties of polyurethane/hyperbranched poly (urea-urethane)-grafted multiwalled carbon nanotube composites', *Composites Part B: Engineering*. Elsevier, 42(8), pp. 2111–2116.